# CEP-stable high-energy ytterbium-doped fiber amplifier

M. Natile, A. Golinelli, L. Lavenu, F. Guichard, Marc Hanna, Y. Zaouter, R. Chiche, X. Chen, J. F Hergott, W. Boutu, et al.

Optics Letters

# CEP-stable high-energy ytterbium-doped fiber amplifier

M. Natile,[1,2,*] A. Golinelli,[3] L. Lavenu,[1,3] F. Guichard,[1] M. Hanna,[3] Y. Zaouter,[1] R. Chiche,[4] X. Chen,[1] J. F. Hergott,[2] W. Boutu,[2] H. Merdji,[2] and P. Georges[3]

[1]Amplitude Laser, 2–4 rue du Bois Chaland CE 2926, 91029 Evry, France
[2]LIDYL, CEA, CNRS, Université Paris-Saclay, UMR 9222 CEA-SACLAY, 91191 Gif-sur-Yvette, France
[3]Laboratoire Charles Fabry, Institut d'Optique Graduate School, CNRS, Université Paris-Saclay, 91127 Palaiseau Cedex, France
[4]Laboratoire de l'Accélérateur Linéaire, IN2P3, CNRS, Université Paris-Saclay, 91898 Orsay Cedex, France
*Corresponding author: michele.natile@amplitude-laser.com

Received 10 April 2019; accepted 10 June 2019; posted 18 June 2019 (Doc. ID 364621); published 5 August 2019

**We report on the carrier-envelope phase (CEP) stabilization of a Yb-doped fiber amplifier system delivering 30 μJ pulses at 100 kHz repetition rate. A single-shot, every-shot measurement of the CEP stability based on a simple f-2f interferometer is performed, yielding a CEP standard deviation of 320 mrad rms over 1 s. Long-term stability is also assessed, with 380 mrad measured over 1 h. This level of performance is allowed by a hybrid architecture, including a passively CEP-stabilized front-end based on difference frequency generation and an active CEP stabilization loop for the fiber amplifier system, acting on a telecom-grade integrated LiNbO3 phase modulator. Together with recent demonstrations of temporal compression down to the few-cycle regime, the presented results demonstrate the relevance of the Yb-doped high repetition rate laser for attoscience.** 

https://doi.org/10.1364/OL.44.003909

Carrier-envelope phase (CEP) stabilized few-cycle amplified laser systems are one of the keys enabling attoscience [1,2]. Since the first demonstration of isolated attosecond pulse generation [3], applications requiring a precise control of the electric field have considerably expanded. To date, titanium-doped sapphire (Ti:Sa) amplifier systems have mostly provided the required short and energetic pulses at repetition rates ranging from 50 Hz to 10 kHz [4,5].

A large number of applications would benefit from further repetition rate scaling to ≥100 kHz, reducing acquisition times and improving signal-to-noise ratio. This is particularly true for low yield experiments involving coincidence detection [6]. At repetition rates above 10 kHz, high-power Ti:Sa amplifiers become complicated and costly, and do not provide the long-term stability and robustness required by today's science. A proposed and demonstrated alternative is using CEP-stable Ti:Sa to seed optical parametric chirped pulse amplifiers (OPCPAs) [7,8]. Of particular interest, OPCPAs can be configured to work at different wavelengths opening new opportunities. However, OPCPAs are limited by the low conversion efficiency from the pump to the useable beam (∼15%) before spatial and temporal distortions occur. Very powerful hence, costly, pump sources have to be employed to generate only a few tens of watts [9]. In the past years, laser sources based on Ytterbium gain material have shown stunning performances with >kilowatt average power and >millijoule energy per pulses [10,11]. Furthermore, efficient nonlinear compression of these laser sources down to the few-cycle regime has been demonstrated [12,13] and used to drive high-photon flux extreme ultraviolet (XUV) sources [14,15] through high-harmonic generation (HHG). However, robust CEP stabilization is still missing. This is due to a number of reasons such as noisy fiber oscillator characteristics [16], a large stretching and compression ratio, and enhanced intensity to CEP noise transfer in different nonlinear stages [17]. To date, CEP stabilization of Ytterbium-based amplified systems have been realized in a linear amplification regime at the microjoule level with a regenerative Yb:KGW system at 1 MHz seeded by a solid-state Yb:KGW oscillator [18] and with a fiber amplifier at 80 MHz seeded by a CEP-stable Ti:Sa oscillator [19]. Both systems revealed CEP fluctuations comparable to Ti:Sa and OPCPA sources, but are not directly scalable in average power for the former one [18] and in pulse energy for the latter one [19]. A CEP-stable Tm-doped linear fiber CPA architecture at 2 μm has also been demonstrated recently [20].

In this Letter, we report, to the best of our knowledge, on the first high-energy CEP-stabilized Yb-doped fiber chirped-pulse amplifier (FCPA) system, including a multi-pass cell (MPC) nonlinear compression stage [21]. It delivers 30 μJ 96 fs pulses at 100 kHz and relies on the following several key elements:

- A passively CEP-stable front-end at a central wavelength of 1030 nm.
- A FCPA system, including preamplifiers, a rod-type fiber power amplifier, and a large stretching/compression ratio.
- An active CEP feedback loop, including an in-line in-focus f-to-2f interferometer and an integrated electro-optic phase modulator (PM) as an actuator.

The CEP stability is characterized in detail both at the full 100 kHz bandwidth over 1 s and at 10 kHz over 1 h, revealing

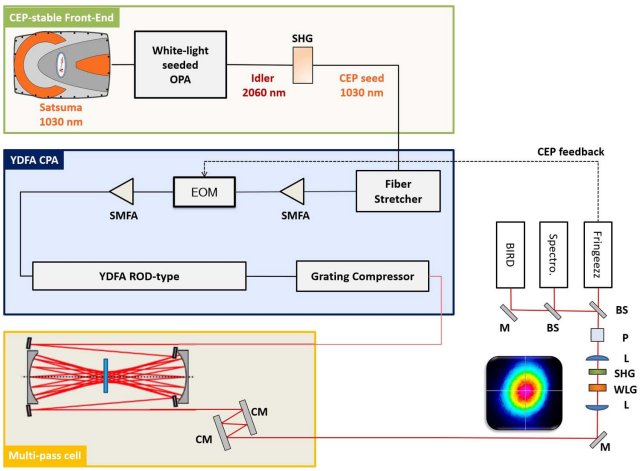


**Fig. 1.** Experimental setup. SHG, second-harmonic generation; WLG, white light generation; OPA, optical parametric amplification; SMFA, single-mode fiber amplifier; EOM, electro-optical modulator; CM, chirped mirror; M, mirror; L, lens; P, polarizer; BS, beam splitter.

<400 mrad CEP stability on a shot-to-shot basis. This is, to the best of our knowledge, the first spectral f-2f CEP measurement ever reported at a repetition rate >10 kHz. Overall, this source demonstrates that Yb-based ultrafast laser technology is compatible with CEP stabilization, paving the way for the future generation of compact and efficient laser drivers for attoscience applications.

The experiment is depicted in Fig. 1. It consists of a passive CEP-stable front-end, seeding a large stretching/compression ratio high-energy FCPA, followed by a MPC temporal compression stage.

The front-end uses a commercially available FCPA (Satsuma, Amplitude Laser) that delivers 40 μJ 300 fs pulses at a repetition rate tunable up to 500 kHz. After second-harmonic generation (SHG) in a 2 mm long BBO crystal with 49% efficiency, this source pumps an optical parametric amplifier (OPA). Both the white light generated signal and OPA pump originate from the same laser pulse train. In this configuration, the idler radiation is inherently CEP-stabilized [22]. Here, the idler wavelength is tuned at 2060 nm and further converted to 1030 nm through a second stage of SHG in a 2 mm long BBO. Up to 400 nJ of energy per pulse is produced and seeded in the FCPA with a full width at half-maximum pulse duration of 185 fs. The repetition rate of the CEP-stable seeder is tunable up to 500 kHz through the control of the OPA pump laser. It is used at 100 kHz throughout this paper. The high-energy FCPA is composed of a chirped fiber Bragg grating stretcher (stretched pulse duration ~350 ps), followed by two single-mode low-power fiber pre-amplifiers that provide a total gain of 26 dB. Between these amplifiers, a waveguide fiber-coupled $LiNbO_3$ PM is inserted (insertion loss of 3 dB) and used as a CEP control device. The possibility to stabilize the CEP of a Ti:Sa amplified laser using a bulk electro-optic modulator was demonstrated in Ref. [23]. The voltage required to shift the CEP phase by $\pi$ is related to the standard $V_\pi$ by

$$V_{\pi,\mathrm{CEP}} = V_\pi \frac{n_e r_{33}}{\lambda\left(3r_{33}\frac{\partial n_e}{\partial \lambda} + n_e \frac{\partial r_{33}}{\partial \lambda}\right)}, \quad (1)$$

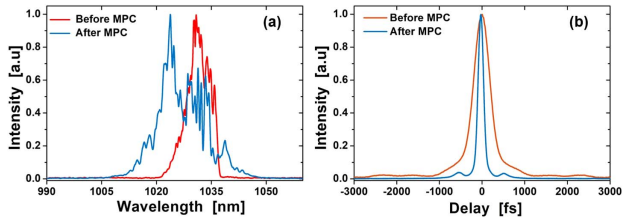


**Fig. 2.** (a) Spectra and (b) autocorrelation traces at the output of the CPA (red) and MPC-based temporal compression (blue).

where $\lambda$ is the wavelength, $n_e$ is the extraordinary refractive index of $LiNbO_3$ and $r_{33}$ is one component of its electro-optic tensor. We estimate the value of the right-hand side fraction in Eq. (1) to be 7, which is consistent with the experimentally measured value of $V_{\pi,\mathrm{CEP}}$ of 8 V, and the specified $V_\pi < 2$ V. The power amplifier is composed of a 1 m long rod-type fiber with a mode field diameter of 65 μm pumped by a high-power 976 nm diode laser nominally used at an average power of 10 W. Finally, a highly dispersive 1750 l/mm 12 cm large grating compressor is set up to compress the pulse down to 340 fs.

Additional temporal compression is performed by means of a bulk MPC. The MPC is made of two spherical mirrors with a radius of curvature of 200 mm, separated by 240 mm. The pulses recirculate for 15 roundtrips in the MPC in which a 2.3 mm thick antireflection-coated silica plate is inserted. Here the role of the MPC is twofold.

First, the pulse duration reduction increases the coherence of the white light generation process for CEP measurement. Secondly, it is included as a test bench to study CEP stability in the presence of a highly nonlinear compression stage that must be included in a future high-power source for attosecond physics.

Figure 2 shows the spectral and temporal characteristics of the pulses at the output of the FCPA and after the MPC. At an input energy to the MPC of 30 μJ, limited by the decreasing output temporal pulse quality, the spectrum is broadened from 16 nm to 45 nm (measured at −10 dB) leading to a pulse duration of 96 fs out of the MPC (assuming a Gaussian shape for the deconvolution), after chirp removal using 4800 $fs^2$ of negative dispersion. The transmission of this stage is 89%.

Finally, an in-line, in-focus f-to-2f interferometer setup is used for CEP characterization [24]. A pulse energy of ~1.5 μJ is sampled out of the MPC beam and focused into a 3 mm thick YAG crystal for octave-spanning spectral broadening. In the same focus, a 2 mm thick BBO crystal is used to frequency double the spectral content in the 1100–1150 nm range, generating the spectral interference pattern in the 550–575 nm range after a polarizing cube.

We now focus on the in-depth characterization of the CEP stability. Three separate devices are used to detect spectral fringes from the f-2f interferometer, allowing us to investigate different properties.

First, a commercial fast CEP measurement device (Fringeezz, Fastlite) is used at the output of the f-to-2f interferometer to acquire single-shot CEP values at a 10 kHz sampling rate. This signal is fed to a digital proportional–integral–derivative (PID) servo-controller that drives the PM. Figure 3(a) shows the in-loop CEP power spectral density (PSD) and RMS integrated phase noise (IPN) in open and closed loop operation, acquired over 10 s. In the closed loop case, an

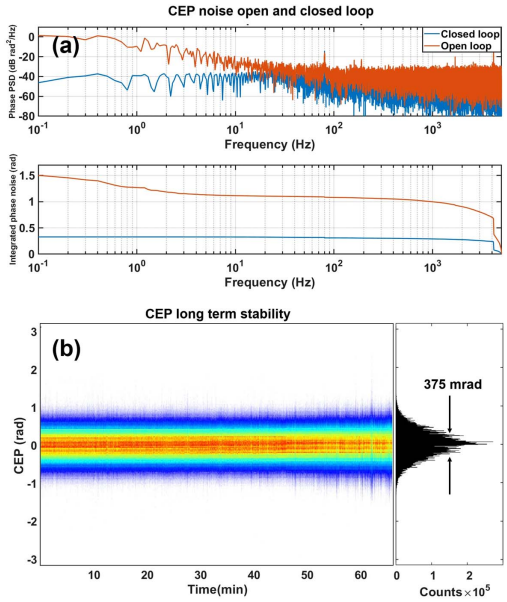


**Fig. 3.** In-loop single-shot CEP characterization at a 10 kHz sampling rate (a) CEP PSD and IPN for open and closed loop operations. (b) Left: the CEP density plot in closed loop over 60 min. Right: corresponding CEP histogram.

overall IPN of 320 mrad is obtained, owing to the strong reduction of low-frequency noise allowed by the feedback loop. A long-term CEP density plot (one histogram per second) over 1 h is also shown in Fig. 3(b) and yields an overall IPN of 375 mrad, demonstrating the robustness of the system.

Secondly, while using the first device to stabilize the CEP out-of-loop characterization is performed by measuring the spectral fringes using a fast spectrometer. The minimum integration time of 30 μs allows us to measure CEP fluctuations integrating over three pulses, at a maximum sampling rate of 330 Hz. Figure 4(a) shows the fringe spectrum acquired on the first acquisition (used to measure the fringe visibility), Fig. 4(b) shows the fringe pattern as a function of time, Fig. 4(c) shows the corresponding CEP variation as a function of time [25], and Fig. 4(d) shows the overall CEP histogram over 3 s for three different integration times of 30 μs, 100 μs, and 1 ms, corresponding, respectively, to 3, 10, and 100 shots averaging. The IPN increases from 56 mrad to 115 mrad and 214 mrad for decreasing integration times, with corresponding noise bandwidths of [0.3 Hz–1 kHz], [0.3 Hz–10 kHz], and [0.3 Hz–33 kHz]. An interesting point is to compare the measured fringe contrast, which is sometimes used as a way to characterize the CEP stability [26]. In our case, it remains essentially constant, with a visibility increasing from 68.3%–68.9% from the less to the most integrated case. Therefore, this visibility is not a meaningful indication of CEP stability in these conditions.

Finally, a third CEP measurement is performed out-of-loop, with a focus on measuring the shot-to-shot CEP at 100 kHz using the Beat Interferometer for Rapid Detection (BIRD, Amplitude Laser) technique [27]. This measurement is completely analog and based on the use of the difference signal from two photomultipliers detecting the signals of a spatially dispersed spectral fringe hitting the apex of a prism. Figure 5(a) shows the closed loop PSD and corresponding IPN on the frequency range [1 Hz–50 kHz]. The total integrated RMS CEP noise is 325 mrad for an acquisition time of 1 s. This measurement confirms the Fringeezz measurement, but over the full bandwidth. To the best of our knowledge, this is the first time that a spectral f-to-2f measurement has been performed at 100 kHz. The only other report of shot-to-shot CEP measurement at 100 kHz that we are aware of is based on stereo above threshold ionization, as reported in Ref. [28].

Lastly, we report on intensity fluctuations of the complete laser source, which are known to be correlated with CEP noise through various amplitude-to-phase noise transfer mechanisms [29,30]. As an example, self-phase modulation in the white light generation (inside the OPA and the f-to-2f), amplification stages, and MPC could cause such a transfer. We characterize

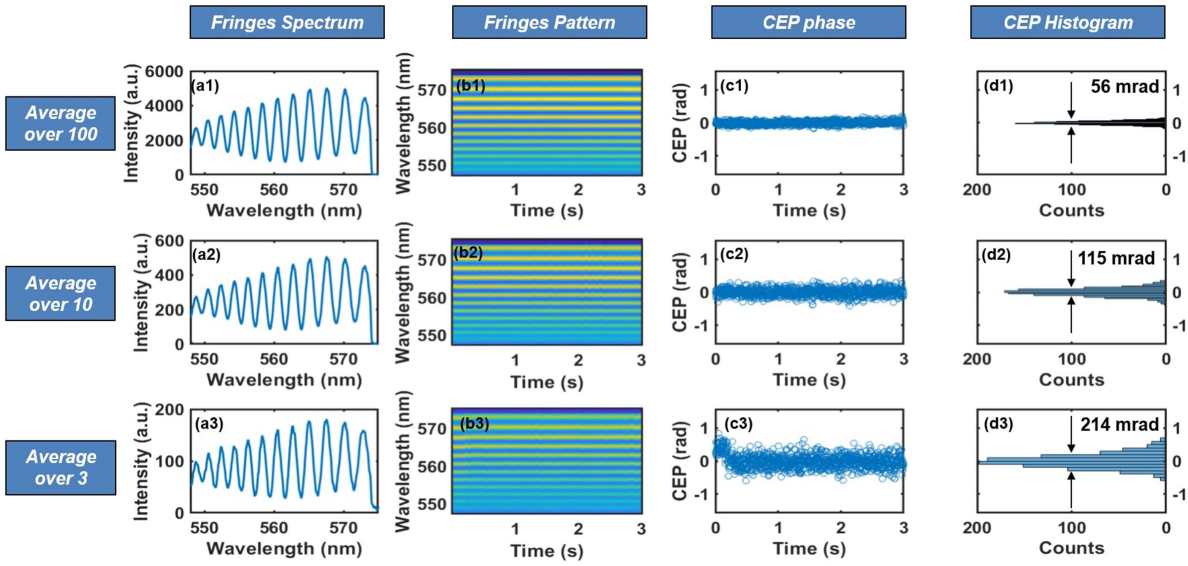


**Fig. 4.** Out-of-loop f-2f spectral fringe measurement with a spectrometer. (a1)–(a3) Single acquisition of spectral fringes with integration times corresponding to 100, 10, and 3 pulses, respectively. (b1)–(b3) Corresponding fringe pattern evolution as a function of time over 3 s. (c1)–(c3) Corresponding CEP drift as a function of time. (d1)–(d3) Histograms of CEP fluctuations.

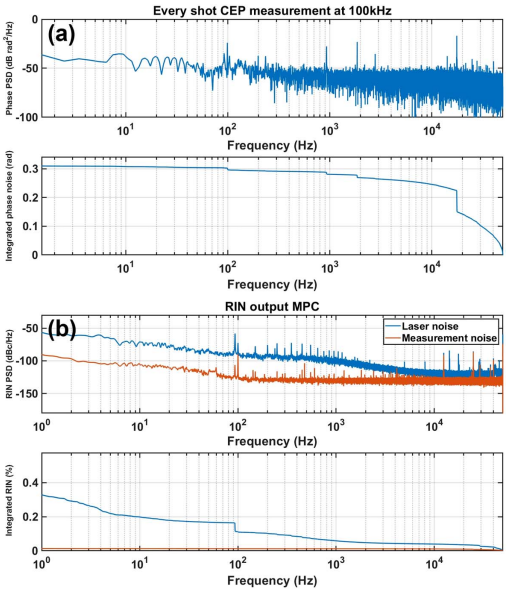


**Fig. 5.** (a) Full PSD and IPN from a single-shot, every-shot measurement. (b) PSD and IRIN at the output of the laser source.

our system in terms of relative intensity noise. The measurement setup consists of a Si photodiode, a low-pass filter at Nyquist frequency, and an oscilloscope. The RIN PSD and integrated RMS RIN (IRIN) measured after the MPC are shown in Fig. 5(b). The total IRIN is 0.32% in the [1 Hz–50 kHz] bandwidth. For reference, the IRIN of the pump laser of the OPA measured in the same conditions is 0.5%, indicating that saturation in the amplifiers throughout the system reduces the IRIN. We also point out a RIN spectral peak at 100 Hz which is clearly correlated to a peak at the same frequency in the CEP PSD [see Fig. 5(a)]. This is clear evidence of an amplitude-to-phase noise transfer. As expected, therefore, a low value of IRIN is paramount in the design of such a CEP-stable system.

In conclusion, we demonstrated the CEP stabilization of an ultrafast FCPA followed by an MPC-based nonlinear temporal compression stage. This proof-of-principle system delivers 30 μJ 96 fs pulses centered at 1030 nm, at a 100 kHz repetition rate with a full-bandwidth single-shot CEP stability better than 400 mrad and RMS IRIN of 0.32%. These results bring clear evidence of the compatibility of all subsystems, including stretcher/compressor units, single-mode fiber amplifiers, large-mode-area power amplifiers, and nonlinear compression in an MPC, with CEP stabilization. Taking into account the already demonstrated high-energy, high-power [11] amplifier architectures, as well as the high-efficiency nonlinear compression schemes [31], the system performances could realistically be scaled. We believe that this Letter paves the way to the development of compact, robust, CEP-stable, high-power (>100 W), high-energy (>500 μJ), few-cycle sources particularly attractive for a wide range of applications such as XUV generation through HHG, attoscience, coincidence spectroscopy, and nanoscale imaging.

**Funding.** Conseil Départemental de l'Essonne (ASTRE Sophie); FP7 People: Marie-Curie Actions (PEOPLE) (H2020-MSCA-ITN-2014-641789-MEDEA); Agence Nationale de la Recherche (ANR) (ANR-10-LABX-0039-PALM).

## REFERENCES

1. F. Krausz and M. Ivanov, Rev. Mod. Phys. **81**, 163 (2009).
2. G. Sansone, L. Poletto, and M. Nisoli, Nat. Photonics **5**, 655 (2011).
3. G. Sansone, E. Benedetti, F. Calegari, C. Vozzi, L. Avaldi, R. Flammini, L. Poletto, P. Villoresi, C. Altucci, R. Velotta, S. Stagira, S. De Silvestri, and M. Nisoli, Science **314**, 443 (2006).
4. G. Gademann, F. Plé, P.-M. Paul, and M. J. Vrakking, Opt. Express **19**, 24922 (2011).
5. J. Klein and J. D. Kafka, Nat. Photonics **4**, 289 (2010).
6. M. Weger, J. Maurer, A. Ludwig, L. Gallmann, and U. Keller, Opt. Express **21**, 21981 (2013).
7. J. Rothhardt, S. Demmler, S. Hädrich, J. Limpert, and A. Tünnermann, Opt. Express **20**, 10870 (2012).
8. O. Chalus, P. K. Bates, M. Smolarski, and J. Biegert, Opt. Express **17**, 3587 (2009).
9. R. Budriūnas, T. Stanislauskas, J. Adamonis, A. Aleknavičius, G. Veitas, D. Gadonas, S. Balickas, A. Michailovas, and A. Varanavičius, Opt. Express **25**, 5797 (2017).
10. M. Müller, M. Kienel, A. Klenke, T. Gottschall, E. Shestaev, M. Plötner, J. Limpert, and A. Tünnermann, Opt. Lett. **41**, 3439 (2016).
11. B. Dannecker, J.-P. Negel, A. Loescher, P. Oldorf, S. Reichel, R. Peters, T. Graf, and M. A. Ahmed, Opt. Commun. **429**, 180 (2018).
12. L. Lavenu, M. Natile, F. Guichard, Y. Zaouter, M. Hanna, E. Mottay, and P. Georges, Opt. Express **25**, 7530 (2017).
13. J. Rothhardt, S. Hädrich, A. Klenke, S. Demmler, A. Hoffmann, T. Gotschall, T. Eidam, M. Krebs, J. Limpert, and A. Tünnermann, Opt. Lett. **39**, 5224 (2014).
14. S. Hädrich, J. Rothhardt, M. Krebs, S. Demmler, A. Klenke, A. Tünnermann, and J. Limpert, J. Phys. B **49**, 172002 (2016).
15. A. I. Gonzalez, G. Jargot, P. Rigaud, L. Lavenu, F. Guichard, A. Comby, T. Auguste, O. Sublemontier, M. Bougeard, Y. Zaouter, P. Georges, M. Hanna, and T. Ruchon, J. Opt. Soc. Am. B **35**, A6 (2018).
16. N. Raabe, T. Feng, M. Mero, H. Tian, Y. Song, W. Hänsel, R. Holzwarth, A. Sell, A. Zach, and G. Steinmeyer, Opt. Lett. **42**, 1068 (2017).
17. F. Lücking, A. Trabattoni, S. Anumula, G. Sansone, F. Calegari, M. Nisoli, T. Oksenhendler, and G. Tempea, Opt. Lett. **39**, 2302 (2014).
18. T. Balčiūnas, T. Flöry, A. Baltuška, T. Stanislauskas, R. Antipenkov, A. Varanavičius, and G. Steinmeyer, Opt. Lett. **39**, 1669 (2014).
19. T. Saule, S. Holzberger, O. De Vries, M. Plötner, J. Limpert, A. Tünnermann, and I. Pupeza, Appl. Phys. B **123**, 17 (2017).
20. C. Gaida, T. Heuermann, M. Gebhardt, E. Shestaev, T. P. Butler, D. Gerz, N. Lilienfein, P. Sulzer, M. Fischer, R. Holzwarth, and A. Leitenstorfer, Opt. Lett. **43**, 5178 (2018).
21. M. Hanna, X. Délen, L. Lavenu, F. Guichard, Y. Zaouter, F. Druon, and P. Georges, J. Opt. Soc. Am. B **34**, 1340 (2017).
22. G. Cerullo, A. Baltuška, O. D. Mücke, and C. Vozzi, Laser Photonics Rev. **5**, 323 (2011).
23. O. Gobert, P. Paul, J. Hergott, O. Tcherbakoff, F. Lepetit, P. D'Oliveira, F. Viala, and M. Comte, Opt. Express **19**, 5410 (2011).
24. M. Kakehata, H. Takada, Y. Kobayashi, K. Torizuka, Y. Fujihira, T. Homma, and H. Takahashi, Opt. Lett. **26**, 1436 (2001).
25. M. Takeda, H. Ina, and S. Kobayashi, J. Opt. Soc. Am. **72**, 156 (1982).
26. C.-H. Lu, T. Witting, A. Husakou, M. J. Vrakking, A. Kung, and F. J. Furch, Opt. Express **26**, 8941 (2018).
27. S. Koke, C. Grebing, B. Manschwetus, and G. Steinmeyer, Opt. Lett. **33**, 2545 (2008).
28. D. Hoff, F. J. Furch, T. Witting, K. Rühle, D. Adolph, A. M. Sayler, M. J. Vrakking, G. G. Paulus, and C. P. Schulz, Opt. Lett. **43**, 3850 (2018).
29. A. Baltuska, M. Uiberacker, E. Goulielmakis, R. Kienberger, V. S. Yakovlev, T. Udem, T. W. Hansch, and F. Krausz, IEEE J. Sel. Top. Quantum Electron. **9**, 972 (2003).
30. C. Li, E. Moon, H. Wang, H. Mashiko, C. M. Nakamura, J. Tackett, and Z. Chang, Opt. Lett. **32**, 796 (2007).
31. L. Lavenu, M. Natile, F. Guichard, X. Délen, M. Hanna, Y. Zaouter, and P. Georges, Opt. Express **27**, 1958 (2019).